

# Dark matter physics in neutrino specific two Higgs doublet model

Seungwon Baek<sup>1,\*</sup> and Takaaki Nomura<sup>1,†</sup>

<sup>1</sup>*School of Physics, KIAS, Seoul 02455, Korea*

(Dated: November 29, 2016)

## Abstract

Although the seesaw mechanism is a natural explanation for the small neutrino masses, there are cases when the Majorana mass terms for the right-handed neutrinos are not allowed due to symmetry. In that case, if neutrino-specific Higgs doublet is introduced, neutrinos become Dirac particles and their small masses can be explained by its small VEV. We show that the same symmetry, which we assume a global  $U(1)_X$ , can also be used to explain the stability of dark matter. In our model, a new singlet scalar breaks the global symmetry spontaneously down to a discrete  $Z_2$  symmetry. The dark matter particle, lightest  $Z_2$ -odd fermion, is stabilized. We discuss the phenomenology of dark matter: relic density, direct detection, and indirect detection. We find that the relic density can be explained by a novel Goldstone boson channel or by resonance channel. In the most region of parameter space considered, the direct detections is suppressed well below the current experimental bound. Our model can be further tested in indirect detection experiments such as FermiLAT gamma ray searches or neutrinoless double beta decay experiments.

Keywords:

---

\*Electronic address: swbaek@kias.re.kr

†Electronic address: nomura@kias.re.kr

## I. INTRODUCTION

A natural scenario to explain the sub-eV neutrino masses is type-I seesaw mechanism in which very heavy standard model (SM) singlet right-handed neutrinos are introduced. In this case the light-neutrinos become Majorana particles and the scenario can be tested at neutrinoless double beta decay experiments.

A more straightforward way for the generation of neutrino masses in parallel with the generation of quark or charged lepton masses is just to introduce right-handed neutrinos to get Dirac neutrino masses with the assumption of lepton number conservation to forbid the Majorana mass terms of the right-handed neutrinos. The problem in this case is the neutrino Yukawa couplings should be tiny ( $\lesssim 10^{-11}$ ) while the top quark Yukawa coupling is of order 1. To give Dirac masses to neutrinos, while avoiding this large hierarchy problem, neutrino-two-Higgs-doublet model ( $\nu$ THDM) was suggested [1]. In this model, the small neutrino masses are explained by the small VEV of a second Higgs doublet ( $v_1 = \sqrt{2}\langle\Phi_1^0\rangle \sim \mathcal{O}(1)$  eV) while the neutrino Yukawa couplings can be of order 1. The authors in Ref. [1] introduced global  $U(1)$  symmetry,  $U(1)_X$ , which is softly broken to forbid Majorana mass terms of the right-handed neutrinos. In their model, all the SM fermions except neutrinos obtain masses via Yukawa interactions with the SM-like Higgs doublet,  $\Phi_2$ , while only neutrinos get masses from Yukawa interaction with  $\Phi_1$ :

$$\mathcal{L}_Y = -\overline{Q}_L Y^u \tilde{\Phi}_2 u_R - \overline{Q}_L Y^d \Phi_2 d_R - \overline{L}_L Y^e \Phi_2 e_R - \overline{L}_L Y^\nu \tilde{\Phi}_1 \nu_R + h.c., \quad (\text{I.1})$$

where  $\tilde{\Phi}_i = i\sigma_2 \Phi_i^*$  ( $i = 1, 2$ ). The  $\Phi_1$  and  $\nu_R$  are assigned with the global charge 1 under  $U(1)_X$ . The global symmetry forbids the Majorana mass term  $\nu_R \nu_R$ . If the global symmetry is *softly* broken by introducing a term in the scalar potential,  $V \ni -m_{12}^2 \Phi_1^\dagger \Phi_2 + h.c.$ , the small VEV is obtained by seesaw-like formulas

$$v_1 = \frac{m_{12}^2 v_2}{M_A^2}, \quad (\text{I.2})$$

where  $M_A$  is the pseudo-scalar mass [1]. For the electroweak scale  $M_A (\sim 100)$  GeV,  $v_1 \sim 1$  eV can be obtained by  $m_{12} \sim \mathcal{O}(100)$  keV.

We extend the model to include a natural dark matter (DM) candidate,  $\psi$ . In our model the global symmetry,  $U(1)_X$ , is *spontaneously* broken down to discrete  $Z_2$  symmetry by VEV of a new singlet scalar,  $S$ . The remnant  $Z_2$  symmetry makes the dark matter

	Scalar Fields			New Fermion	
	$\Phi_1$	$\Phi_2$	$S$	$\nu_R$	$\psi$
$SU(2)_L$	<b>2</b>	<b>2</b>	<b>1</b>	<b>1</b>	<b>1</b>
$U(1)_Y$	$\frac{1}{2}$	$\frac{1}{2}$	0	0	0
$U(1)_X$	2	0	2	2	1

TABLE I: Scalar fields and new fermion in our model where  $\nu_R$  is Majorana type while  $\psi$  is Dirac type.

candidate stable. The resulting Goldstone boson provides a new annihilation channel for the DM relic density. It is feebly coupled to the SM particles due to tiny  $v_1$ , avoiding experimental constraints. We also study the DM direct detection and indirect detection. They are typically well below the current experimental sensitivity.

The paper is organized as follows. In Section II, we introduce our model. In Section III, we study DM phenomenology in our model: relic abundance, direct and indirect detection of the DM. In Section IV, we conclude.

## II. THE MODEL

In this section, we introduce our model which is an extension of the model given in Ref. [1]. The scalar field contents and new fermions are summarized in Table. I where we also show the charge assignments under global  $U(1)_X$  symmetry. We can write  $U(1)_X$ -invariant as well as the SM-gauge invariant scalar potential, Yukawa interactions for the leptons and new fields as

$$\begin{aligned}
V(\Phi_1, \Phi_2, S) = & -m_{11}^2 \Phi_1^\dagger \Phi_1 - m_{22}^2 \Phi_2^\dagger \Phi_2 - m_S^2 S^\dagger S - (\mu \Phi_1^\dagger \Phi_2 S + h.c.) \\
& + \lambda_1 (\Phi_1^\dagger \Phi_1)^2 + \lambda_2 (\Phi_2^\dagger \Phi_2)^2 + \lambda_3 \Phi_1^\dagger \Phi_1 \Phi_2^\dagger \Phi_2 + \lambda_4 \Phi_1^\dagger \Phi_2 \Phi_2^\dagger \Phi_1 + \lambda_S (S^\dagger S)^2 \\
& + \lambda_{1S} \Phi_1^\dagger \Phi_1 S^\dagger S + \lambda_{2S} \Phi_2^\dagger \Phi_2 S^\dagger S,
\end{aligned} \tag{II.1}$$

$$\mathcal{L} \supset -y_{ij}^e \bar{L}_i \Phi_2 e_{Rj} - y_{ij}^\nu \bar{L}_i \tilde{\Phi}_1 \nu_{Rj} + h.c., \tag{II.2}$$

$$\mathcal{L} \supset \bar{\psi} i \gamma^\mu \partial_\mu \psi - m_\psi \bar{\psi} \psi - \frac{f}{2} \bar{\psi}^c \psi S^\dagger - \frac{f^*}{2} \bar{\psi} \psi^c S. \tag{II.3}$$

Thus Dirac masses of neutrinos are generated by VEV of  $\Phi_1$  which is assumed to be much

smaller than electroweak scale to obtain tiny neutrino mass [1]. In addition, a  $Z_2$  symmetry remains when  $U(1)_X$  is broken by non-zero VEVs of  $S$ . Note that only  $\psi$  is  $Z_2$  odd particle while other particles including those in SM sector are even under the  $Z_2$ , guaranteeing stability of  $\psi$ . Thus  $\psi$  can be a DM candidate in the model.

The scalar fields can be written by

$$\Phi_1 = \begin{pmatrix} \phi_1^+ \\ \frac{1}{\sqrt{2}}(v_1 + h_1 + ia_1) \end{pmatrix}, \quad \Phi_2 = \begin{pmatrix} \phi_2^+ \\ \frac{1}{\sqrt{2}}(v_2 + h_2 + ia_2) \end{pmatrix}, \quad S = \frac{1}{\sqrt{2}}r_S e^{i\frac{a_S}{v_S}}. \quad (\text{II.4})$$

Note that we write  $S$  in terms of radial field  $r_S = v_S + \rho$  and phase field  $a_S$  with  $\langle a_S \rangle = 0$  [6] since  $a_S$  becomes physical Goldstone boson as shown below. The VEVs of the scalar fields are obtained by requiring  $\partial V(v_1, v_2, v_S)/\partial v_i = 0$  which provides following conditions:

$$-2m_{11}^2 v_1 + 2\lambda_1 v_1^3 + v_1(\lambda_{1S} v_S^2 + \lambda_3 v_2^2 + \lambda_4 v_2^2) - \sqrt{2}\mu v_2 v_S = 0, \quad (\text{II.5})$$

$$-2m_{22}^2 v_2 + 2\lambda_2 v_2^3 + v_2(\lambda_{2S} v_S^2 + \lambda_3 v_1^2 + \lambda_4 v_1^2) - \sqrt{2}\mu v_1 v_S = 0, \quad (\text{II.6})$$

$$-2m_{SS}^2 v_S + 2\lambda_S v_S^3 + v_S(\lambda_{1S} v_1^2 + \lambda_{2S} v_2^2) - \sqrt{2}\mu v_1 v_2 = 0. \quad (\text{II.7})$$

We then find that these conditions can be satisfied with  $v_1 \simeq \mu \ll \{v_2, v_S\}$  and SM Higgs VEV is given as  $v \simeq v_2 \simeq 246$  GeV. From (II.5) we find that  $v_1$  is proportional to and of the same order with  $\mu$ :

$$v_1 \simeq \frac{\sqrt{2}\mu v_2 v_S}{\lambda_{1S} v_S^2 + (\lambda_3 + \lambda_4) v_2^2 - 2m_{11}^2}. \quad (\text{II.8})$$

We note that small  $\mu \ll v$  is technically natural [2, 3] because  $\mu \equiv 0$  enhances the symmetry of the Lagrangian (II.1) to additional  $U(1)$  under which only the  $S$  field is charged while all the others are neutral.

Here we consider masses and mass eigenstate of the scalar sector by analyzing the scalar potential with  $v_1 \sim \mu \ll \{v_2, v_S\}$ .

*Pseudo-scalar* : Mass matrix for pseudo-scalars is given, in the basis of  $(a_1, a_2, a_S)$ , by

$$M_A^2 \simeq \frac{\mu}{\sqrt{2}} \begin{pmatrix} \frac{v_2 v_S}{v_1} & -v_S & -v_2 \\ -v_S & \frac{v_1 v_S}{v_2} & v_1 \\ -v_2 & v_1 & 0 \end{pmatrix} \simeq \begin{pmatrix} \frac{\mu v_2 v_S}{\sqrt{2} v_1} & 0 & 0 \\ 0 & 0 & 0 \\ 0 & 0 & 0 \end{pmatrix}, \quad (\text{II.9})$$

where we used  $S \simeq (v_S + \rho + ia_S)/\sqrt{2}$  to obtain the mass matrix. We thus find three mass eigenstates  $A$ ,  $a$ , and  $G_0$ :  $A(\simeq a_1)$  is massive pseudo-scalar,  $a(\simeq a_S)$  is physical

massless Goldstone boson associated with  $U(1)_X$  breaking as indicated above, and  $G_0(\simeq a_2)$  is massless Nambu-Goldstone (NG) boson which is absorbed by  $Z$  boson. The mass of  $A$  is given by

$$m_A^2 = \frac{\mu(v_1^2 v_2^2 + v_1^2 v_S^2 + v_2^2 v_S^2)}{\sqrt{2}v_1 v_2 v_S} \simeq \frac{\mu v_2 v_S}{\sqrt{2}v_1}. \quad (\text{II.10})$$

Note that the existence of physical Goldstone boson  $a$  does not lead to serious problems in particle physics or cosmology since it does not couple to SM particles directly except to SM Higgs. Invisible decay width of  $Z$ -boson strongly constrains the  $Z \rightarrow H_i a$  decay<sup>1</sup>. Since  $v_S$  is a free parameter, we can make  $\rho$  (or the mass eigenstate with  $\rho$  as main component) heavier than the  $Z$ -boson mass to evade the problem [4]. In our model,  $a$  can couple also to electron via  $ig_{\bar{e}ea} a \bar{e}\gamma_5 e$  interaction through mixing with the SM Higgs doublet. Stellar energy loss constrains  $g_{\bar{e}ea} \lesssim 10^{-12}$  model-independently [5]. The tree-level contribution in our model,  $g_{\bar{e}ea} \simeq m_e v_1 / (v v_S) \approx 2 \times 10^{-16} (v_1 / 1 \text{ eV}) (100 \text{ GeV} / v_S)$ , satisfies the bound safely.

Our model can also contribute about 0.39 to the effective number of neutrino species  $\Delta N_{\text{eff}}$  [6] when  $\lambda_{2S} = 0.005$  and  $m_{H_3} = 500 \text{ MeV}$ . This can solve [7, 8] about  $3.4\sigma$  discrepancy between Hubble Space Telescope [7] and Plank [9] in the measurement of Hubble constant. Since the mechanism is almost the same with that detailed in [6] we do not further discuss implication of the Goldstone boson on  $\Delta N_{\text{eff}}$ .

*Charged scalar* : For charged scalar case, mass matrix in the basis of  $(\phi_1^\pm, \phi_2^\pm)$  is given by

$$M_{H^\pm}^2 = \begin{pmatrix} \frac{v_2(\sqrt{2}\mu v_S - \lambda_4 v_1 v_2)}{2v_1} & -\frac{1}{2}(\sqrt{2}\mu v_S - \lambda_4 v_1 v_2) \\ -\frac{1}{2}(\sqrt{2}\mu v_S - \lambda_4 v_1 v_2) & \frac{v_1(\sqrt{2}\mu v_S - \lambda_4 v_1 v_2)}{2v_2} \end{pmatrix} \simeq \begin{pmatrix} \frac{v_2(\sqrt{2}\mu v_S - \lambda_4 v_1 v_2)}{2v_1} & 0 \\ 0 & 0 \end{pmatrix}, \quad (\text{II.11})$$

which indicates that  $\phi_1^\pm$  is approximately physical charged scalar,  $H^\pm$ , and  $\phi_2^\pm$  is approximately  $G^\pm$ , the NG boson absorbed by  $W^\pm$  boson. We obtain the charged Higgs mass as

$$m_{H^\pm}^2 = \frac{(v_1^2 + v_2^2)(\sqrt{2}\mu v_S - \lambda_4 v_1 v_2)}{2v_1 v_2} \simeq \frac{v_2(\sqrt{2}\mu v_S - \lambda_4 v_1 v_2)}{2v_1}. \quad (\text{II.12})$$

*CP-even scalar* : In the case of CP-even scalar, all three components are physical, and the

---

<sup>1</sup>  $H_i (i = 1, 2, 3)$  are neutral scalars defined below.

mass matrix in the basis of  $(h_1, h_2, \rho)$  is written as

$$M_H^2 = \begin{pmatrix} 2\lambda_1 v_1^2 + \frac{\mu v_2 v_S}{\sqrt{2} v_1} & (\lambda_3 + \lambda_4) v_1 v_2 - \frac{\mu v_S}{\sqrt{2}} & \lambda_{1S} v_1 v_S - \frac{\mu v_2}{\sqrt{2}} \\ (\lambda_3 + \lambda_4) v_1 v_2 - \frac{\mu v_S}{\sqrt{2}} & 2\lambda_2 v_2^2 + \frac{\mu v_1 v_S}{\sqrt{2} v_2} & \lambda_{2S} v_2 v_S - \frac{\mu v_1}{\sqrt{2}} \\ \lambda_{1S} v_1 v_S - \frac{\mu v_2}{\sqrt{2}} & \lambda_{2S} v_2 v_S - \frac{\mu v_1}{\sqrt{2}} & 2\lambda_S v_S^2 + \frac{\mu v_1 v_2}{\sqrt{2} v_S} \end{pmatrix} \\ \simeq \begin{pmatrix} \frac{\mu v_2 v_S}{\sqrt{2} v_1} & 0 & 0 \\ 0 & 2\lambda_2 v_2^2 & \lambda_{2S} v_2 v_S \\ 0 & \lambda_{2S} v_2 v_S & 2\lambda_S v_S^2 \end{pmatrix}. \quad (\text{II.13})$$

We find that all the masses of the mass eigenstates,  $H_i (i = 1, 2, 3)$ , are at the electroweak scale and the mixings between  $h_1$  and other components are negligibly small while the  $h_2$  and  $\rho$  can have sizable mixing. The mass eigenvalue and mixing angle for  $h_2$  and  $\rho$  system are given by

$$m_{H_2, H_3}^2 = \frac{1}{2} \left[ m_{22}^2 + m_{33}^2 \mp \sqrt{(m_{22}^2 - m_{33}^2)^2 + 4m_{23}^4} \right], \quad (\text{II.14})$$

$$\tan 2\theta = \frac{-2m_{23}^2}{m_{22}^2 - m_{33}^2}, \quad (\text{II.15})$$

$$m_{22}^2 = 2\lambda_2 v_2^2, \quad m_{33}^2 = 2\lambda_S v_S^2, \quad m_{23}^2 = \lambda_{2S} v_2 v_S. \quad (\text{II.16})$$

Then mass eigenstates are obtained as

$$\begin{pmatrix} H_1 \\ H_2 \\ H_3 \end{pmatrix} \simeq \begin{pmatrix} 1 & 0 & 0 \\ 0 & \cos \theta & -\sin \theta \\ 0 & \sin \theta & \cos \theta \end{pmatrix} \begin{pmatrix} h_1 \\ h_2 \\ \rho \end{pmatrix} \quad (\text{II.17})$$

Note that  $H_2$  is the SM-like Higgs,  $h$ , and  $m_{H_2} \simeq m_h$  where mixing angle  $\theta$  is constrained to be  $\sin \theta \lesssim 0.2$  by data of Higgs search at the LHC [10–13]. For small mixing, we have  $H_2 \simeq h$  and  $H_3 \simeq \rho$ . In addition, we take into account constraint from  $h \rightarrow aa$  decay which is induced by interaction term  $1/(v_S) \rho \partial_\mu a \partial^\mu a$  from kinetic term of  $S$ . The decay width can be estimated as

$$\Gamma_{h \rightarrow aa} = \frac{\sin^2 \theta}{16\pi} \left( \frac{m_h}{v_S} \right)^2 m_h, \quad (\text{II.18})$$

and we require upper limit of the branching ratio as  $BR(h \rightarrow aa) < 0.23$  based on constraint of invisible decay of SM Higgs [14–16]. The phenomenology of two Higgs doublet sector is discussed in Ref. [1] in detail. We thus focus on DM physics in the following analysis.

*Dark sector* : To obtain interactions of  $\psi$  and physical scalar bosons, we define a field  $\psi'$  by [6]

$$\psi = \psi' e^{i \frac{a_S}{2v_S}}, \quad (\text{II.19})$$

so that the direct coupling of  $a_S$  to  $\psi'$  disappears. Then the Lagrangian for  $\psi'$  becomes

$$\mathcal{L} \supset \bar{\psi}' i \gamma^\mu \partial_\mu \psi' - m_\psi \bar{\psi}' \psi' - \frac{1}{2v_S} \bar{\psi}' \gamma^\mu \psi' \partial_\mu a_S - \frac{f}{2\sqrt{2}} \bar{\psi}'^c \psi' r_S - \frac{f}{2\sqrt{2}} \bar{\psi}' \psi'^c r_S, \quad (\text{II.20})$$

where  $f$  is taken to be real and positive by an appropriate choice of phase of  $\psi$ . Since  $r_S (= v_S + \rho)$  has non-zero VEV, the mass eigenstates of  $Z_2$  odd fermions are obtained as a pair of self-charge-conjugate fields;

$$\psi_+ = \frac{1}{\sqrt{2}} (\psi' + \psi'^c), \quad \psi_- = \frac{-i}{\sqrt{2}} (\psi' - \psi'^c), \quad (\text{II.21})$$

which satisfy Majorana conditions  $\psi_\pm^c = \psi_\pm$  and have mass eigenvalues

$$m_\pm = m_\psi \pm \frac{fv_S}{\sqrt{2}}. \quad (\text{II.22})$$

Thus  $\psi_-$  is our DM candidate in the following analysis. Finally the Lagrangian for the mass eigenstates is given by

$$\begin{aligned} \mathcal{L} \supset & \frac{1}{2} \sum_{\alpha=\pm} \bar{\psi}_\alpha [i \gamma^\mu \partial_\mu - m_\pm] \psi_\alpha - \frac{i}{4v_S} [\bar{\psi}_+ \gamma^\mu \psi_- - \bar{\psi}_- \gamma^\mu \psi_+] \partial_\mu a_S \\ & - \frac{f}{2\sqrt{2}} \rho [\bar{\psi}_+ \psi_+ - \bar{\psi}_- \psi_-]. \end{aligned} \quad (\text{II.23})$$

### III. DARK MATTER PHYSICS

In this section, we discuss DM physics such as relic density, direct detection and indirect detection. Our DM candidate is the new Majorana fermion  $\psi_-$  which is stable due to  $Z_2$  symmetry as a remnant of the global  $U(1)_X$  symmetry. Interactions relevant to DM physics are obtained from the kinetic term of  $S$ , terms in Eq. (II.1), and (II.20):

$$\begin{aligned} \mathcal{L} \supset & - \frac{f}{2\sqrt{2}} \rho (\bar{\psi}_+ \psi_+ - \bar{\psi}_- \psi_-) - \frac{i}{4v_S} [\bar{\psi}_+ \gamma^\mu \psi_- - \bar{\psi}_- \gamma^\mu \psi_+] \partial_\mu a \\ & - \mu_{SS} \rho^3 + \frac{1}{v_S} \rho \partial_\mu a \partial^\mu a - \mu_{1S} \rho \left( \phi_1^+ \phi_1^- + \frac{1}{2} (h_1^2 + a_1^2) \right) - \frac{\mu_{2S}}{2} \rho h_2^2, \end{aligned} \quad (\text{III.1})$$

where we defined  $\mu_{SS} \equiv \lambda_S v_S$ ,  $\mu_{1S} \equiv \lambda_{1S} v_S$  and  $\mu_{2S} \equiv \lambda_{2S} v_S$ , and  $\rho(h_2)$  can be written in terms of mass eigenstates via Eq. (II.17). In the following analysis, we consider four different

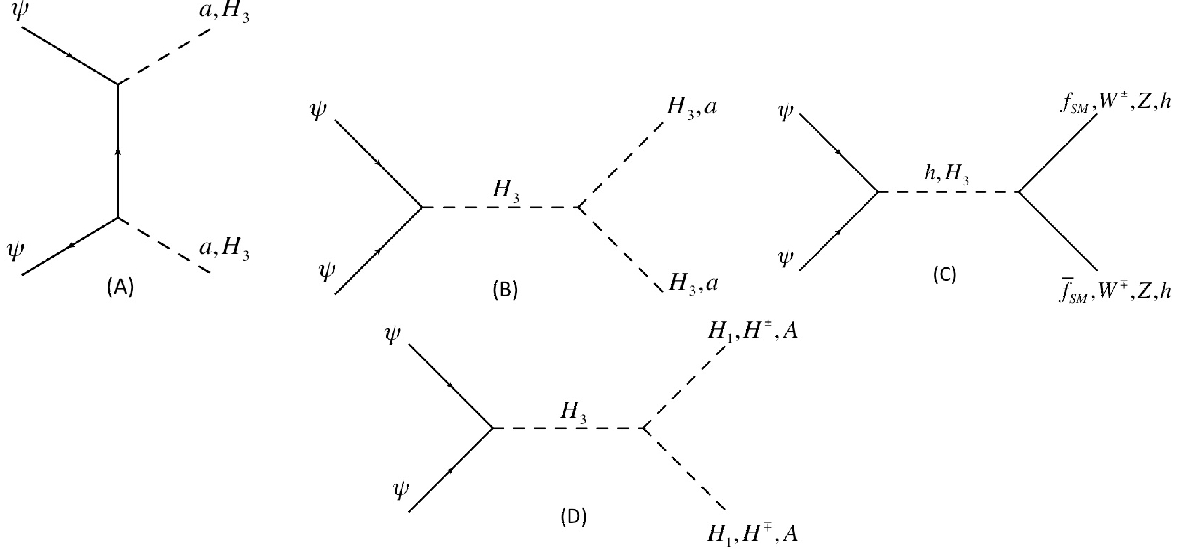


FIG. 1: The DM annihilation processes.

scenarios for the coupling constants: (I)  $f \leq \sqrt{4\pi}$  and  $\mu_{1S,2S,SS} \ll 0.1$  GeV, (II)  $f \leq \sqrt{4\pi}$  and  $\mu_{SS} \gg \mu_{1S,2S}$ , (III)  $f \leq 0.8$  and  $\mu_{2S} \gg \mu_{1S,SS}$ , (IV)  $f \leq 0.8$  and  $\mu_{1S} \gg \mu_{2S,SS}$ . For scenario (I), DM dominantly annihilate into  $\rho\rho$  and/or  $aa$  via interaction with coupling  $f$  as Fig. 1-(A) [6, 17–19] and  $aa$  via process in Fig. 1-(B). In the scenario (II), final states of DM annihilation process is same as scenario (I) where  $\psi_+\psi_- \rightarrow H_3 \rightarrow H_3 H_3$  mode in Fig. 1-(B) is added. In the scenarios (III) and (IV), a DM pair dominantly annihilates via s-channel processes where  $\rho(\simeq H_3)$  propagates as an intermediate particle; the dominant final states are, depending on parameters,  $\{hh, f_{SM}f_{SM}, W^+W^-, ZZ\}$  and  $\{H_1H_1, AA, H^+H^-\}$  for the scenarios (III) and (IV) respectively as shown in Fig. 1 (C) and (D), and  $aa$  channel in Fig. 1-(B) which contributes to both scenarios. Note that,  $\mu_{2S}$  induces mixing between  $h_2$  and  $\rho$  and we discuss constraint from direct detection taking into account Higgs portal interaction [20–26] with the mixing effect for scenario (III).

### A. Relic density

We estimate the thermal relic density of DM numerically using `micrOMEGAs 4.3.1` [27] to solve the Boltzmann equation by implementing relevant interactions inducing the DM pair annihilation processes. Then we search for parameter sets which satisfy the approximate



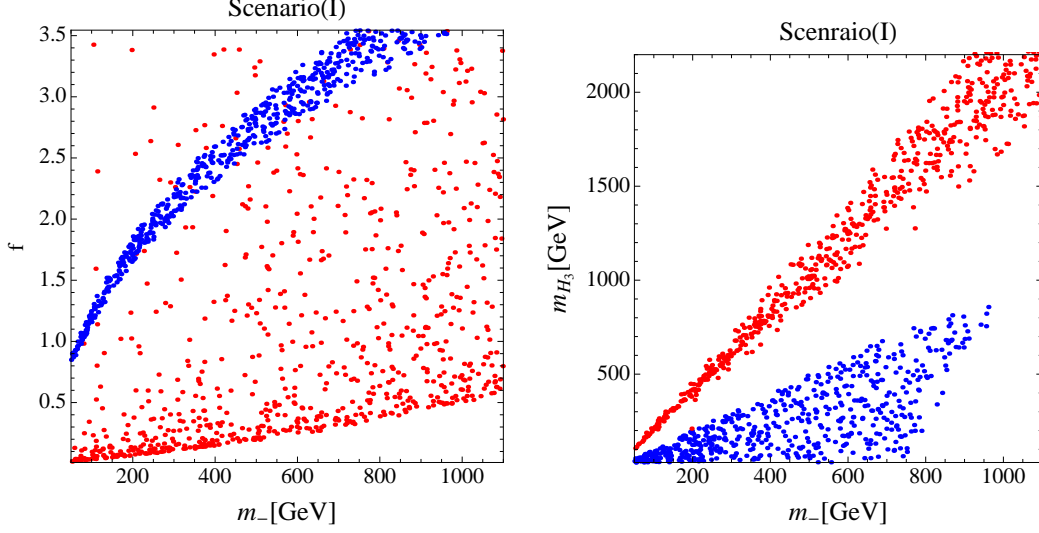


FIG. 2: The parameter points providing required relic density of DM in scenario (I) where red and blue points correspond to the case of  $m_- + m_+ > m_{H_3} > m_-$  and  $m_- > m_{H_3}$  respectively.

region for the relic density [28]

$$0.11 \lesssim \Omega h^2 \lesssim 0.13. \quad (\text{III.2})$$

In numerical calculations random parameter sets are prepared in the following parameter ranges for each scenario:

$$\text{For all scenario : } m_- \in [50, 1100] \text{ GeV}, \quad m_{H_3} \in [30, 2200], \quad v_S = 1000 \text{ GeV}, \quad (\text{III.3})$$

$$\text{scenario (I) : } f \in [0.1, \sqrt{4\pi}], \quad \mu_{1S} = \mu_{2S} = \mu_{SS} = 10^{-3} \text{ GeV}, \quad (\text{III.4})$$

$$\text{scenario (II) : } f \in [0.01, \sqrt{4\pi}], \quad \mu_{SS} \in [0.1, m_{H_3}] \text{ GeV}, \quad \mu_{1S} = \mu_{2S} = 10^{-3} \text{ GeV}, \quad (\text{III.5})$$

$$\text{scenario (III) : } f \in [0.01, 0.8], \quad \mu_{2S} \in [0.1, m_{H_3}] \text{ GeV}, \quad \mu_{1S} = \mu_{SS} = 10^{-3} \text{ GeV}, \quad (\text{III.6})$$

$$\begin{aligned} \text{scenario (IV) : } f \in [0.01, 0.8], \quad \mu_{1S} \in [0.1, m_{H_3}] \text{ GeV}, \quad \mu_{2S} = \mu_{SS} = 10^{-3} \text{ GeV}, \\ m_{H_1} = m_{H^\pm} = m_A \in [70, m_\psi] \text{ GeV}, \end{aligned} \quad (\text{III.7})$$

where we assumed  $m_{H_1} = m_{H^\pm} = m_A$  for simplicity and they are taken to be larger than  $m_\psi$  in scenario (I) to (III).

In Fig. 2, we show parameter points which explain the observed relic density of DM for scenario (I) where red and blue points correspond to the case of (a)  $m_- + m_+ > m_{H_3} > m_-$  and (b)  $m_- > m_{H_3}$ . We find that the case of  $m_{H_3} > m_- + m_+$  cannot provide observed

relic density with  $f < \sqrt{4\pi}$  since only  $\psi_{\pm}\psi_{\pm} \rightarrow aa$  channel is allowed. In the case (a),  $\psi_{-}\psi_{-} \rightarrow H_3 \rightarrow aa$  in Fig. 1-(B) dominates and the region near resonance,  $m_{H_3} \sim 2m_{-}$ , is preferred as shown in the right plot of Fig. 2. Also in the case (a), for smaller  $f$ ,  $t$ -channel coannihilation process  $\psi_{-}\psi_{+} \rightarrow H_3 a$  is enhanced near threshold  $m_{H_3} \simeq m_{-} + m_{+}$  due to the  $t$ -channel propagator of  $\psi_{\pm}$  contributes  $1/(m_{+}^2 - m_{-}^2)$  factor to the amplitude. In the case (b), the relevant process is coannihilation  $\psi_{-}\psi_{+} \rightarrow H_3 a$  as well as  $\psi_{-}\psi_{-} \rightarrow H_3 H_3, aa$ , shown in Fig. 1-(A),(B). The case (a) allows wide parameter space than the case (b) in the  $(m_{-}, f)$ -plane simply due to resonance dominance in the case (a).

We find that the allowed parameter points for scenario (II) is similar to scenario (I) since new contribution from the process  $\psi_{-}\psi_{-} \rightarrow H_3 \rightarrow H_3 H_3$  is subdominant. The allowed region in  $(m_{-}, f)$ -plane becomes slightly wider due to new contribution for  $m_{-} > m_{H_3}$  while most of  $\mu_{SS}$  region can be allowed. Since the result is similar to that of scenario (I) we omit the plot for scenario (II).

The allowed parameter points for scenario (III) and (IV) are given in Fig. 3 in  $(m_{-}, \mu_{2S(1S)})$ - and  $(m_{-}, m_{H_3})$ -plane. We find that parameter space with  $m_{H_3} \sim 2m_{-}$  as can be seen from Fig. 1-(C) and (D) can explain the relic density since resonant enhancement is required to achieve sufficient annihilation cross section. For the resonant region, wide range of  $\mu_{2S(1S)}$  is allowed as shown in left plots of Fig. 3. For scenario (III), parameter space with large value of  $\mu_{2S}$  is constrained by constraint from mixing angle  $\sin \theta < 0.2$  and invisible decay branching ratio of SM Higgs. In addition, larger resonant enhancement is required to obtain sufficient annihilation cross section. In scenario (IV), also dependence on the value of  $m_{H_1}$  is small unless it is not very close to that of  $m_{-}$ .

## B. Direct detection

Here we discuss direct detection of DM in our model focusing on our scenario (III) since  $\rho$ - $h_2$  mixing is negligibly small in other scenarios. The DM-nucleon scattering is induced by the SM Higgs exchanging process via mixing effect in scalar sector in our model, which is calculated in non-relativistic limit. We obtain the following effective Lagrangian by integrating out  $h$  and  $H_3$ ;

$$\mathcal{L}_{\text{eff}} = \sum_q \frac{f m_q s_{\theta} c_{\theta}}{2\sqrt{2}v} \left( \frac{1}{m_h^2} - \frac{1}{m_{H_3}^2} \right) \bar{\psi}_{-}\psi_{-}\bar{q}q \quad (\text{III.8})$$

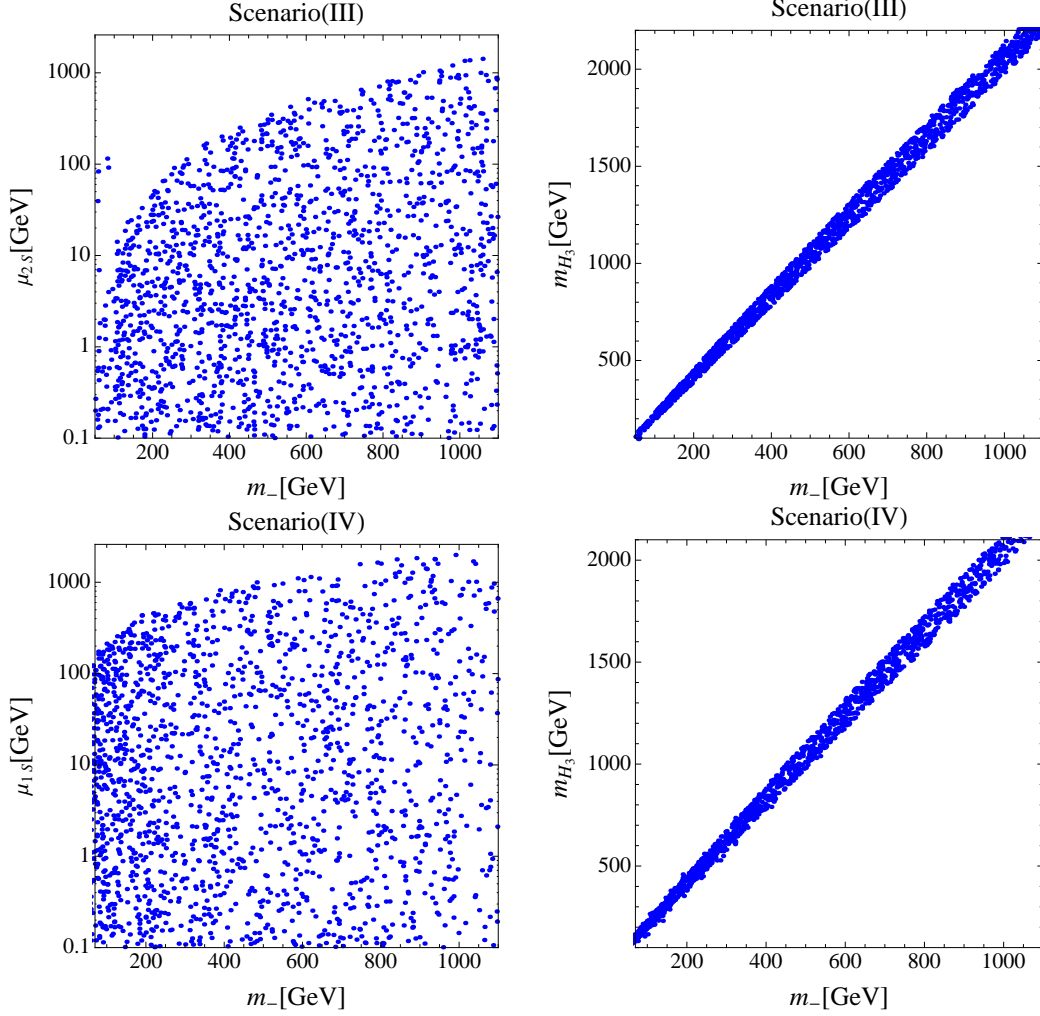


FIG. 3: The parameter points providing required relic density of DM in scenarios (II) and (III) on the  $m_\psi$ - $\mu_{SS(2S)}$  plane (left plot) and the  $m_\psi$ - $m_{H_3}$  plane (right plot).

where  $s_\theta(c_\theta) = \sin\theta(\cos\theta)$ ,  $q$  and  $m_q$  denote the corresponding quark field and the quark mass respectively, and the sum is over all quark flavors. The effective Lagrangian can be rewritten as  $\psi$ -nucleon (N) interaction:

$$\mathcal{L}_{\text{eff}} = \frac{f_N m_N f s_\theta c_\theta}{2\sqrt{2}v} \left( \frac{1}{m_h^2} - \frac{1}{m_{H_3}^2} \right) \bar{\psi}_- \psi_- \bar{N} N, \quad (\text{III.9})$$

where the effective coupling constant  $f_N$  is obtained by

$$f_N = \sum_q f_q^N = \sum_q \frac{m_q}{m_N} \langle N | \bar{q} q | N \rangle. \quad (\text{III.10})$$

Here we replace the heavy quark contribution by the gluon contributions such that [24]

$$\sum_{q=c,b,t} f_q^N = \frac{1}{m_N} \sum_{q=c,b,t} \langle N | \left( -\frac{\alpha_s}{12\pi} G_{\mu\nu}^a G^{a\mu\nu} \right) | N \rangle, \quad (\text{III.11})$$

which is obtained by calculating the triangle diagram. The trace of the stress energy tensor is written as follows by considering the scale anomaly;

$$\theta_\mu^\mu = m_N \bar{N} N = \sum_q m_q \bar{q} q - \frac{7\alpha_s}{8\pi} G_{\mu\nu}^a G^{a\mu\nu}. \quad (\text{III.12})$$

Combining Eqs. (III.11) and (III.12), we obtain

$$\sum_{q=c,b,t} f_q^N = \frac{2}{9} \left( 1 - \sum_{q=u,d,s} f_q^N \right), \quad (\text{III.13})$$

which provides

$$f_N = \frac{2}{9} + \frac{7}{9} \sum_{q=u,d,s} f_q^N. \quad (\text{III.14})$$

Finally the spin independent  $\psi$ - $N$  scattering cross section is given by [29]

$$\sigma_{\text{SI}}(\psi N \rightarrow \psi N) = \frac{1}{2\pi} \frac{\mu_{N\psi}^2 f_N^2 m_N^2 f_\theta^2 s_\theta^2 c_\theta^2}{v^2} \left( \frac{1}{m_h^2} - \frac{1}{m_{H_3}^2} \right)^2 \quad (\text{III.15})$$

where  $m_N$  is the nucleon mass and  $\mu_{N\psi} = m_N m_- / (m_N + m_-)$  is the reduced mass of nucleon and DM. For simplicity, we estimate DM-neutron scattering cross section since that of DM-proton is almost the same. In this case, we apply  $f_n \simeq 0.287$  (with  $f_u^n = 0.0110$ ,  $f_d^n = 0.0273$ ,  $f_s^b = 0.0447$ ) for the sum of the contributions of partons to the mass fraction of neutron [30]. The Fig. 4 shows the DM-nucleon scattering cross section for the allowed parameter sets in scenario (III); for other scenarios the cross section is negligibly small due to small mixing angle  $\theta$ . We find that the cross section is mostly smaller than current constraint from LUX [31] (few parameter space is excluded), and some parameter sets would be tested in future direct detection experiments [32].

### C. Indirect detection

Here we discuss possibility of indirect detection in our model. The thermally averaged cross section in current Universe is estimated with `micrOMEGAs 4.3.1` applying allowed

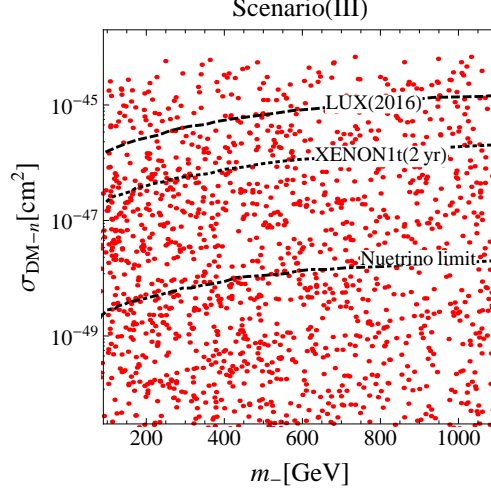


FIG. 4: The DM-nucleon scattering cross section for scenario (III) which is compared with current constraint by LUX [31] and future prospect by XENON 1t [32].

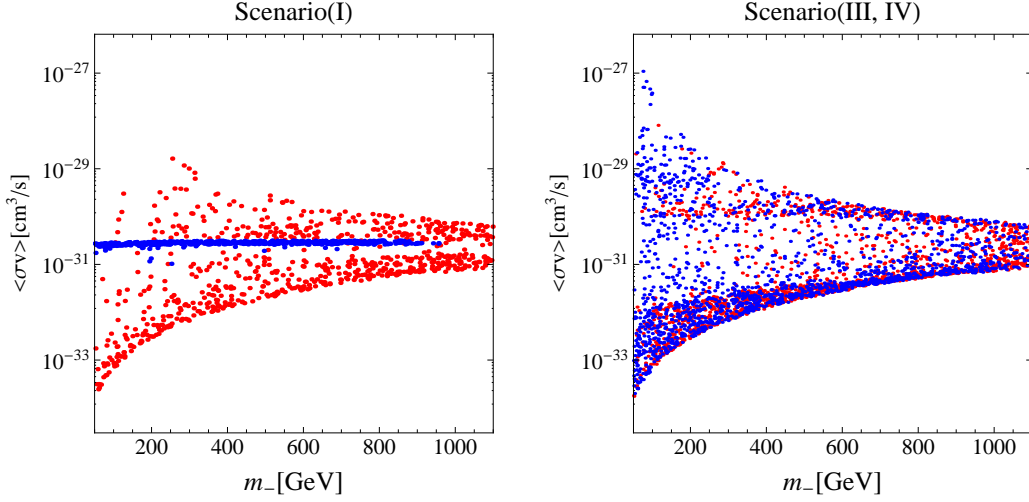


FIG. 5: The thermally averaged DM annihilation cross section at current Universe for parameter sets which provides observed relic density. In the left plot, colors of points correspond to that in Fig. 2. In the right plot, red and blue points correspond to scenario (III) and (IV) respectively.

parameter sets. The Fig. 5 shows the cross section for scenario (I) and scenarios (III,IV) in left and right panel respectively; the scenario (II) provide same feature as scenario (I) and the corresponding plot is omitted here.

For scenario (I), colors of points correspond to that of in Fig. 2. We find that the cross section is suppressed since the amplitude of the process decreases as momentum of

DM decreases. The cross section for  $\psi_-\psi_- \rightarrow H_3H_3$  does not change much while that for  $\psi_-\psi_- \rightarrow H_3a(aa)$  has wide range of value since resonant region  $m_{H_3} \sim 2m_-$  is required in the latter case and the current cross section can be much different from that in freeze out era; the case of  $m_{H_3} \simeq (\lesssim)2m_-$  induce large Breit-Wigner enhancement while the case of  $m_{H_3} \gtrsim 2m_-$  does not induce large enhancement and the cross section is suppressed as the amplitude decreases as DM momentum. The  $H_3$  further decays into  $hh$  and SM particles via the effect of mixing with SM Higgs which lead  $\gamma$ -ray spectrum. Since the cross section is small,  $\gamma$ -ray flux is free from current constraint and the  $\gamma$ -ray spectrum depends on decay pattern of  $H_3$  and detailed analysis is beyond the scope of this paper. The scenario (II) provide same result as scenario (I) since annihilation processes are almost same.

For scenario (III) and (IV), the  $s$ -channel processes with  $\mu_{2S}$  and  $\mu_{1S}$  can be also enhanced. The process  $\psi_-\psi_- \rightarrow H_3 \rightarrow \{hh\}$  is  $\lesssim 10^{-28}\text{cm}^2/s$  due to constraint on  $\mu_{2S}$  from mixing with  $H_3$  and SM Higgs. Note that due to resonant enhancement the cross section can be  $\sim 10^{-27}\text{cm}^2/s$  for the processe  $\psi_-\psi_- \rightarrow H_3 \rightarrow \{H_1H_1, AA, H^+H^-\}$  with  $m_- \lesssim 150$  GeV in scenario (IV) which can be tested by  $\gamma$ -ray search experiments such as Fermi-LAT [33] since  $H^\pm$  decay into charged leptons. The decays of  $\{H_1, A, H^\pm\}$  also provide neutrino flux, which is much smaller than current constraint by High energy neutrino search such as IceCube [34, 35], and It would be tested in future observation.

#### IV. CONCLUSIONS AND DISCUSSIONS

We have studied a dark matter model in which neutrinos get Dirac masses. The global  $U(1)_X$  symmetry forbids the Majorana mass terms of the right-handed neutrinos, thereby allowing the Dirac masses for the neutrinos. The same symmetry, broken down to a discrete  $Z_2$  symmetry, guarantees the stability of a dark matter candidate which is a hidden sector fermion charged under the global  $U(1)_X$ . The spontaneous symmetry breaking of  $U(1)_X$  occurs due to VEV,  $v_S$ , of a hidden sector scalar  $S$  whose pseudo-scalar component becomes Goldstone boson, providing a new channel to the DM annihilations.

We considered four scenarios depending on the size of coupling constants,  $f$ ,  $\lambda_{SS}v_S$ ,  $\lambda_{2S}v_S$ , and  $\lambda_{1S}v_S$  which regulate the interaction strength of DM and  $S$ , self-coupling of  $S$ , SM Higgs and  $S$ , and scalar doublet for neutrinos and  $S$ , respectively. In scenario (I), we assumed  $f$  can be large while suppressing  $\lambda_{SS}v_S$ ,  $\lambda_{2S}v_S$ , and  $\lambda_{1S}v_S$ . In scenarios (II), (III),

(IV), we suppressed  $f < 0.8$ , allowing large  $\lambda_{SS}v_S$ ,  $\lambda_{2S}v_S$ , and  $\lambda_{1S}v_S$ , respectively.

In scenarios (I) and (II), depending on the DM mass, coupling  $f \gtrsim 0.05$  can explain the current DM relic abundance. In scenarios (III) and (IV), the DM relic density can be accommodated near the resonance,  $2m_- \approx m_{H_3}$ , where the DM annihilation cross section is enhanced.

Only scenario (III) has tree-level contribution to the direct detection via dark-scalar mixing with the SM Higgs boson. Even in this case the direct detection cross section is marginal or well below the current LUX bound due to small mixing as observed at the LHC.

We also investigated the implications of our model on the indirect detection of DM. In scenarios (I) and (II), the channels,  $\psi_-\psi_- \rightarrow \{aH_3, H_3H_3\}$ , are suppressed because the amplitude is momentum-dependent while the channel  $\psi_-\psi_- \rightarrow aa$  can be sizable due to Breit-Wigner enhancement. However,  $aa$  channel can not be detected by the observation. In scenario (III), the cross section for  $hh$  channel is suppressed due to constraint from  $H_3$  and SM mixing. On the other hand, In scenario (IV), with resonant enhancement the annihilation cross section for  $hh$  and  $\{H_1H_1, H^+H^-, AA\}$  can be,  $\langle\sigma v\rangle \gtrsim 10^{-27} \text{ cm}^3/\text{s}$ , for  $m_\psi \lesssim 150 \text{ GeV}$  which is in the ballpark of the sensitivity of experiments such as Fermi-LAT when scalar bosons decay into charged fermions.

## Acknowledgments

This work is supported in part by National Research Foundation of Korea (NRF) Research Grant NRF-2015R1A2A1A05001869 (SB).

- 
- [1] S. M. Davidson and H. E. Logan, Phys. Rev. D **80**, 095008 (2009) [arXiv:0906.3335 [hep-ph]].
  - [2] G. 't Hooft, “Naturalness, chiral symmetry, and spontaneous chiral symmetry breaking”, Proceedings of the 1979 Cargèse Institute on Recent Developments in Gauge Theories, G. 't Hooft, *et. al.* eds., Plenum Press, New York, U.S.A (1980).
  - [3] S. Baek, JHEP **1508** (2015) 023 [arXiv:1410.1992 [hep-ph]].
  - [4] P. H. Frampton, M. C. Oh and T. Yoshikawa, Phys. Rev. D **66** (2002) 033007 [hep-ph/0204273].

- [5] D. Chang, W. Y. Keung and P. B. Pal, Phys. Rev. Lett. **61** (1988) 2420.
- [6] S. Weinberg, Phys. Rev. Lett. **110**, no. 24, 241301 (2013) [arXiv:1305.1971 [astro-ph.CO]].
- [7] A. G. Riess *et al.*, Astrophys. J. **826** (2016) no.1, 56 [arXiv:1604.01424 [astro-ph.CO]].
- [8] P. Ko and Y. Tang, Phys. Lett. B **762** (2016) 462 [arXiv:1608.01083 [hep-ph]].
- [9] P. A. R. Ade *et al.* [Planck Collaboration], Astron. Astrophys. **594** (2016) A13 [arXiv:1502.01589 [astro-ph.CO]].
- [10] The numerical analyses on the Higgs decays are performed using the program HDECAY: A. Djouadi, J. Kalinowski and M. Spira, Comput. Phys. Commun. 108 (1998) 56; A. Djouadi, M. Muhlleitner and M. Spira, Acta. Phys. Polon. B38 (2007) 635.
- [11] S. Choi, S. Jung and P. Ko, JHEP **1310**, 225 (2013) [arXiv:1307.3948 [hep-ph]].
- [12] K. Cheung, P. Ko, J. S. Lee and P. Y. Tseng, JHEP **1510**, 057 (2015) [arXiv:1507.06158 [hep-ph]].
- [13] K. Cheung, P. Ko, J. S. Lee, J. Park and P. Y. Tseng, Phys. Rev. D **94**, no. 3, 033010 (2016) [arXiv:1512.07853 [hep-ph]].
- [14] G. Aad *et al.* [ATLAS Collaboration], JHEP **1601**, 172 (2016) [arXiv:1508.07869 [hep-ex]].
- [15] G. Aad *et al.* [ATLAS Collaboration], JHEP **1511** (2015) 206 [arXiv:1509.00672 [hep-ex]].
- [16] V. Khachatryan *et al.* [CMS Collaboration], arXiv:1610.09218 [hep-ex].
- [17] M. Lindner, D. Schmidt and T. Schwetz, Phys. Lett. B **705** (2011) 324 [arXiv:1105.4626 [hep-ph]].
- [18] S. Baek, P. Ko, H. Okada and E. Senaha, JHEP **1409** (2014) 153 [arXiv:1209.1685 [hep-ph]].
- [19] S. Baek and H. Okada, Phys. Lett. B **728** (2014) 630 [arXiv:1311.2380 [hep-ph]].
- [20] Y. G. Kim, K. Y. Lee and S. Shin, JHEP **0805** (2008) 100 [arXiv:0803.2932 [hep-ph]].
- [21] S. Baek, P. Ko and W. I. Park, JHEP **1202** (2012) 047 [arXiv:1112.1847 [hep-ph]].
- [22] S. Baek, P. Ko and W. I. Park, JHEP **1307** (2013) 013 [arXiv:1303.4280 [hep-ph]].
- [23] S. Baek, P. Ko, W. I. Park and E. Senaha, JHEP **1305** (2013) 036 [arXiv:1212.2131 [hep-ph]].
- [24] S. Baek, P. Ko and W. I. Park, Phys. Rev. D **90** (2014) no.5, 055014 [arXiv:1405.3530 [hep-ph]].
- [25] C. H. Chen and T. Nomura, Phys. Lett. B **746**, 351 (2015) [arXiv:1501.07413 [hep-ph]].
- [26] S. Baek, T. Nomura and H. Okada, Phys. Lett. B **759** (2016) 91 [arXiv:1604.03738 [hep-ph]].
- [27] G. Belanger, F. Boudjema, A. Pukhov and A. Semenov, arXiv:1407.6129 [hep-ph].
- [28] P. A. R. Ade *et al.* [Planck Collaboration], Astron. Astrophys. (2014) [arXiv:1303.5076 [astro-]]



- ph.CO]].
- [29] J. Hisano, R. Nagai and N. Nagata, JHEP **1505** (2015) 037 [arXiv:1502.02244 [hep-ph]].
  - [30] G. Belanger, F. Boudjema, A. Pukhov and A. Semenov, Comput. Phys. Commun. **185**, 960 (2014) [arXiv:1305.0237 [hep-ph]].
  - [31] D. S. Akerib *et al.*, arXiv:1608.07648 [astro-ph.CO].
  - [32] E. Aprile *et al.* [XENON Collaboration], JCAP **1604**, no. 04, 027 (2016) [arXiv:1512.07501 [physics.ins-det]].
  - [33] M. Ackermann *et al.* [Fermi-LAT Collaboration], Phys. Rev. Lett. **115**, no. 23, 231301 (2015) [arXiv:1503.02641 [astro-ph.HE]].
  - [34] R. Abbasi *et al.* [IceCube Collaboration], Phys. Rev. D **84** (2011) 022004 [arXiv:1101.3349 [astro-ph.HE]].
  - [35] M. G. Aartsen *et al.* [IceCube Collaboration], arXiv:1309.7007 [astro-ph.HE].